Natalie Waksmanski
Department of Civil Engineering,
University of Akron,
Akron, OH 44325-3905
e-mail: npw5@zips.uakron.edu

Ernian Pan[1]
Fellow ASME
Department of Civil Engineering,
University of Akron,
Akron, OH 44325-3905
e-mail: pan2@uakron.edu

Lian-Zhi Yang
College of Science, College of Engineering,
China Agricultural University,
Beijing 100083, China
e-mail: ylz_xiaozhu@126.com

Yang Gao
College of Science,
China Agricultural University,
Beijing 100083, China
e-mail: gaoyangg@gmail.com

Free Vibration of a Multilayered One-Dimensional Quasi-Crystal Plate

An exact closed-form solution of free vibration of a simply supported and multilayered one-dimensional (1D) quasi-crystal (QC) plate is derived using the pseudo-Stroh formulation and propagator matrix method. Natural frequencies and mode shapes are presented for a homogenous QC plate, a homogenous crystal plate, and two sandwich plates made of crystals and QCs. The natural frequencies and the corresponding mode shapes of the plates show the influence of stacking sequence on multilayered plates and the different roles phonon and phason modes play in dynamic analysis of QCs. This work could be employed to further expand the applications of QCs especially if used as composite materials.
[DOI: 10.1115/1.4027632]

Keywords: free vibration, 1D quasi-crystals, sandwich plate

1 Introduction

From the diffraction image of rapidly cooled Al–Mn alloys, Shechtman et al. discovered quasi-crystals (QCs) in 1982 [1]. This discovery was revolutionary and showed that QCs exhibit symmetries that are forbidden in classical crystallography. Crystal structures have periodically repeating unit cells that completely fill space and must have two-fold, three-fold, four-fold, or six-fold rotational symmetry. On the contrary, QCs can be both ordered and nonperiodic which form patterns that completely fill space but lack translational symmetry. Since 1980s, several hundred alloys with thermodynamic stability have been found to exhibit quasi-crystalline behavior [2].

Attributing to their nonperiodic atomic structure, QCs possess properties, such as corrosion resistivity, low thermal conductivity, low coefficients of friction, low porosity, high hardness, and high wear resistance. These properties have enabled QCs to be applied as thin films and coatings [2]. Since QCs are hard and brittle at room temperature [2,3], the linear elastic theory established by Ding et al. [4] can be employed to analyze the mechanical properties of QCs. Due to the complicated nature of QC elastic equations, the majority of work is limited to the defect analysis in QC, such as dislocations and cracks under static deformation [3,5–7].

A 1D QC refers to a three-dimensional (3D) structure with atomic arrangement quasi-periodically in one direction and periodically in the plane perpendicular to that direction. While dynamic analysis of crystals has been studied extensively, including damping effects [8], static and transient bending of 1D QC plates were only recently studied [9]. Although various plane fracture dynamic analyses for QCs were conducted [5–7], and free vibration and elastic wave problems were analyzed for other layered structures [10,11], free vibration of 1D QC layered plates in 3D finite space has not been reported in literature, to the best of the authors' knowledge. Therefore, in this work, we derive the exact closed-form solutions of free vibration for 3D layered plates made of 1D QCs and crystals under laterally simply supported conditions. The pseudo-Stroh formalism [12] and the propagator matrix method [13] are utilized to obtain the natural frequencies and mode shapes of 1D QCs layered plates. As numerical illustrations, the normalized natural frequencies of homogeneous crystal and QC plates and sandwich plates composed of QCs and crystals with different stacking sequences are presented. This work could be applied to analyze composites with QC layer(s) and further expand the applications of QCs.

2 Fundamental Equations

In this section, we describe the fundamentals of linear elastic theory for QCs. The displacement field in classical crystals is the phonon displacement field u_i $(i = 1,2,3)$. In QCs, the phason displacement field w_i is introduced to describe the rearrangement of atomic configurations along the quasi-periodic direction. Both displacement fields are needed in the analysis of QCs and they are actually coupled with each other [4,5].

Based on the linear elastic theory of QCs [4], the strain–displacement relations are given by

$$\begin{aligned} \varepsilon_{ij} &= \frac{1}{2}\left(\frac{\partial u_i}{\partial x_j} + \frac{\partial u_j}{\partial x_i}\right) \\ w_{ij} &= \frac{\partial w_i}{\partial x_j} \end{aligned} \tag{1}$$

where ε_{ij} is the phonon strain tensor and w_{ij} is the phason strain tensor. The phonon strain tensor is symmetric, whereas the phason strain tensor is asymmetric.

The generalized constitutive relations of quasi-crystalline material are written as [4]

$$\begin{aligned} \sigma_{ij} &= C_{ijkl}\varepsilon_{kl} + R_{ijkl}w_{kl} \\ H_{ij} &= R_{klij}\varepsilon_{kl} + K_{ijkl}w_{kl} \end{aligned} \tag{2}$$

where σ_{ij} is the phonon stress tensor, C_{ijkl} phonon elastic constants, H_{ij} phason stress tensor, K_{ijkl} phason elastic constants, R_{ijkl} phonon–phason coupling elastic constants, and repeated indices indicate the summation from 1 to 3. It should be noted that although for 1D QCs the phonon stress tensor is symmetric $(\sigma_{ij} = \sigma_{ji})$, the phason stress tensor is not $(H_{ij} \neq H_{ji})$ [5].

[1]Corresponding author.

Contributed by the Technical Committee on Vibration and Sound of ASME for publication in the Journal of Vibration and Acoustics. Manuscript received January 24, 2014; final manuscript received March 25, 2014; published online June 2, 2014. Assoc. Editor: Michael Leamy.

The elastic constants in Eq. (2) depend on the crystal system and Laue class. Particularly for 1D QC, there are 31 possible point groups which are organized into six crystal systems and ten Laue classes [14]. In this work, the hexagonal system and Laue class 10 with point groups 62_h2_h, $6mm$, $\bar{6}m2_h$, and $6/m_hmm$ are considered. For this Laue class, there are five independent phonon elastic constants, two independent phason elastic constants, and three independent phonon–phason coupling elastic constants.

Referring to the Cartesian coordinate system (x_1, x_2, x_3), we consider a 1D hexagonal QC plate with x_1-axis and x_2-axis in the periodic directions and x_3-axis in the quasi-periodic direction. Accordingly, $w_1 = w_2 = 0$. Thus, in terms of this coordinate system, the linear constitutive relations Eq. (2) for 1D hexagonal QC are reduced to [5]

$$\begin{aligned}
\sigma_{11} &= C_{11}\varepsilon_{11} + C_{12}\varepsilon_{22} + C_{13}\varepsilon_{33} + R_1 w_{33} \\
\sigma_{22} &= C_{12}\varepsilon_{11} + C_{11}\varepsilon_{22} + C_{13}\varepsilon_{33} + R_1 w_{33} \\
\sigma_{33} &= C_{13}\varepsilon_{11} + C_{13}\varepsilon_{22} + C_{33}\varepsilon_{33} + R_2 w_{33} \\
\sigma_{23} &= \sigma_{32} = 2C_{44}\varepsilon_{23} + R_3 w_{32} \\
\sigma_{13} &= \sigma_{31} = 2C_{44}\varepsilon_{13} + R_3 w_{31} \\
\sigma_{12} &= \sigma_{21} = 2C_{66}\varepsilon_{12} \\
H_{31} &= 2R_3\varepsilon_{13} + K_2 w_{31} \\
H_{32} &= 2R_3\varepsilon_{23} + K_2 w_{32} \\
H_{33} &= R_1\varepsilon_{11} + R_1\varepsilon_{22} + R_2\varepsilon_{33} + K_1 w_{33}
\end{aligned} \tag{3}$$

with $C_{66} = (C_{11} - C_{12})/2$.

In the absence of body forces, the dynamic equations of motion are governed by [5]

$$\begin{aligned}
\frac{\partial \sigma_{ij}}{\partial x_j} &= \rho \frac{\partial^2 u_i}{\partial t^2} \\
\frac{\partial H_{ij}}{\partial x_j} &= \rho \frac{\partial^2 w_i}{\partial t^2}
\end{aligned} \tag{4}$$

where ρ is the density of the material. The first equation of motion in Eq. (4) is related to phonon modes and will produce three independent equations. For QCs, there exist several theories to describe the dynamic behavior of phasons. The second equation of motion in Eq. (4), derived by Ding et al. [4], follows Bak's [15] model, where phasons are represented by wave propagation. Bak [15] also claims that the structural disorders or structural fluctuations characterize phasons. Another well-known model, presented by Lubensky et al. [16], considers phason modes to be diffusive with a large diffusive time. Accordingly, the large diffusive time is attributed to the insensitivity of phasons to spatial translation [16]. Among the various dynamic theories for QCs, there also exists a combination of these two theories as was adopted by Fan et al. [7]. Even though the unusual behavior of phasons presents many challenges and different points of view in the field, each theory offers valuable insight. Bak's theory, however, is more frequently utilized due to its simplicity [5].

3 Problem Description

We consider an N-layered 1D QC plate as shown in Fig. 1. The origin of the coordinate system is at one of the four corners on the bottom surface such that the plate thickness is in the positive x_3-direction. The dimensions of the plate are $x_1 \times x_2 \times x_3 = L_1 \times L_2 \times H$ and its four lateral sides are simply supported. It is also obvious that layer j has its lower and upper interfaces at $x_3 = x_3^{(j)}$ and $x_3 = x_3^{(j+1)}$, respectively. Accordingly, the thickness of layer j is written as

$$h_j = x_3^{(j+1)} - x_3^{(j)} \tag{5}$$

It follows that $x_3^{(1)} = 0$ and $x_3^{(N+1)} = H$. Along the interface of the layers, it is assumed that the displacement and traction vectors are continuous.

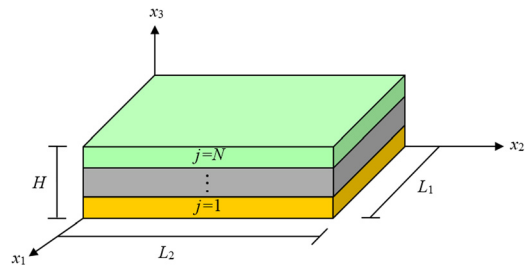

Fig. 1 *N*-layered QC plate

For time-dependent harmonic motion, the solution for phonon and phason displacements under simply supported lateral boundary conditions can be assumed as

$$\boldsymbol{u} = \begin{Bmatrix} u_1 \\ u_2 \\ u_3 \\ w_3 \end{Bmatrix} = e^{sx_3 + i\omega t} \begin{Bmatrix} a_1 \cos px_1 \sin qx_2 \\ a_2 \sin px_1 \cos qx_2 \\ a_3 \sin px_1 \sin qx_2 \\ a_4 \sin px_1 \sin qx_2 \end{Bmatrix} \tag{6}$$

where

$$p = n\pi/L_1 \quad q = m\pi/L_2$$

n and m are positive integers, ω the frequency, s the eigenvalue to be determined, and a_1, a_2, a_3, and a_4 are coefficients to be determined. The solution in Eq. (6) represents only one part of a double Fourier series expansion with summations for n and m over suitable ranges. Thus, whenever the periodic terms appear, summation is implied.

By substituting the solution in Eq. (6) into the general strain–displacement relations, Eq. (1), and subsequently into the constitutive relations, Eq. (3), the traction vector with respect to the x_3 direction is found to be

$$\boldsymbol{t} = \begin{Bmatrix} \sigma_{13} \\ \sigma_{23} \\ \sigma_{33} \\ H_{33} \end{Bmatrix} = e^{sx_3 + i\omega t} \begin{Bmatrix} b_1 \cos px_1 \sin qx_2 \\ b_2 \sin px_1 \cos qx_2 \\ b_3 \sin px_1 \sin qx_2 \\ b_4 \sin px_1 \sin qx_2 \end{Bmatrix} \tag{7}$$

The two vectors

$$\boldsymbol{a} = \{a_1, a_2, a_3, a_4\}^t, \quad \boldsymbol{b} = \{b_1, b_2, b_3, b_4\}^t \tag{8}$$

with the superscript t indicating vector or matrix transpose, are introduced to represent the coefficients in Eqs. (6) and (7), respectively. It can be shown that the coefficient vector $\boldsymbol{b}$ in Eq. (7) can be expressed in terms of the coefficient vector $\boldsymbol{a}$ in Eq. (6) by

$$\boldsymbol{b} = (s\boldsymbol{T} - \boldsymbol{R}^t)\boldsymbol{a} \tag{9}$$

where

$$\begin{aligned}
\boldsymbol{T} &= \begin{bmatrix} C_{44} & 0 & 0 & 0 \\ 0 & C_{44} & 0 & 0 \\ 0 & 0 & C_{33} & R_2 \\ 0 & 0 & R_2 & K_1 \end{bmatrix} \\
\boldsymbol{R} &= \begin{bmatrix} 0 & 0 & C_{13}p & R_1 p \\ 0 & 0 & C_{13}q & R_1 q \\ -C_{44}p & -C_{44}q & 0 & 0 \\ -R_3 p & -R_3 q & 0 & 0 \end{bmatrix}
\end{aligned} \tag{10}$$

Substituting Eq. (6) into Eq. (4), the following simplified equations are obtained:

$$
\begin{aligned}
&-a_1C_{11}p^2 - a_1C_{66}q^2 - a_2C_{12}pq - a_2C_{66}pq + a_1\rho\omega^2 \\
&\quad + s(a_3C_{13}p + a_3C_{44}p + a_4R_1p + a_4R_3p) + a_1C_{44}s^2 = 0 \\
&\quad - a_1C_{12}pq - a_1C_{66}pq - a_2C_{66}p^2 - a_2C_{11}q^2 + a_2\rho\omega^2 \\
&\quad + s(a_3C_{13}q + a_3C_{44}q + a_4R_1q + a_4R_3q) + a_2C_{44}s^2 = 0 \\
&\quad - a_3C_{44}p^2 - a_3C_{44}q^2 - a_4R_3p^2 - a_4R_3q^2 + a_3\rho\omega^2 \\
&\quad - s(a_1C_{13}p + a_1C_{44}p + a_2C_{13}q + a_2C_{44}q) \\
&\qquad + s^2(a_3C_{33} + a_4R_2) = 0 \\
&\quad - a_3R_3p^2 - a_3R_3q^2 - a_4K_2p^2 - a_4K_2q^2 + a_4\rho\omega^2 \\
&\quad - s(a_1R_1p + a_1R_3p + a_2R_1q + a_2R_3q) + s^2(a_4K_1 + a_3R_2) = 0
\end{aligned}
\tag{11}
$$

These equations further simplify to

$$
\left(\boldsymbol{Q} + s(\boldsymbol{R} - \boldsymbol{R}^t) + s^2\boldsymbol{T}\right)\boldsymbol{a} = 0 \tag{12}
$$

where

$$
\boldsymbol{Q} = \begin{bmatrix} -(C_{11}p^2 + C_{66}q^2) + \rho\omega^2 & -pq(C_{12} + C_{66}) & 0 & 0 \\ -pq(C_{12} + C_{66}) & -(C_{66}p^2 + C_{11}q^2) + \rho\omega^2 & 0 & 0 \\ 0 & 0 & -C_{44}(p^2 + q^2) + \rho\omega^2 & -R_3(p^2 + q^2) \\ 0 & 0 & -R_3(p^2 + q^2) & -K_2(p^2 + q^2) + \rho\omega^2 \end{bmatrix} \tag{13}
$$

The formulation in Eq. (12) is similar to the Stroh formalism [17,18]. Thus, it can be appropriately named as the pseudo-Stroh formalism [12].

Using the relation between vectors $\boldsymbol{a}$ and $\boldsymbol{b}$ as indicated by Eq. (9), Eq. (12) can be recast into the following 8×8 linear eigenproblem:

$$
\boldsymbol{N}\begin{Bmatrix} \boldsymbol{a} \\ \boldsymbol{b} \end{Bmatrix} = s\begin{Bmatrix} \boldsymbol{a} \\ \boldsymbol{b} \end{Bmatrix} \tag{14}
$$

where

$$
\mathbf{N} = \begin{bmatrix} \boldsymbol{T}^{-1}\boldsymbol{R}^t & \boldsymbol{T}^{-1} \\ -\boldsymbol{Q} - \boldsymbol{R}\boldsymbol{T}^{-1}\boldsymbol{R}^t & -\boldsymbol{R}\boldsymbol{T}^{-1} \end{bmatrix} \tag{15}
$$

Solving the eigenproblem in Eq. (14) yields eight eigenvalues s_i (for $i = 1, 2, \ldots, 8$). The first four eigenvalues are ordered to have positive real parts. In the case where the real part of the eigenvalue is zero, the positive imaginary portion is taken. The next four eigenvalues have opposite signs of the first four. The eigenvectors corresponding to the eigenvalues s_i follow the same order and make up the vectors $\boldsymbol{a}$ and $\boldsymbol{b}$ [13].

Then the general solution for the displacement vector Eq. (6) and traction vector Eq. (7), with the harmonic time-dependent $i\omega t$ factor omitted for simplicity, is obtained as

$$
\begin{Bmatrix} \boldsymbol{u} \\ \boldsymbol{t} \end{Bmatrix} = \begin{bmatrix} \boldsymbol{A}_1 & \boldsymbol{A}_2 \\ \boldsymbol{B}_1 & \boldsymbol{B}_2 \end{bmatrix} \langle e^{s^* x_3} \rangle \begin{Bmatrix} \boldsymbol{D}_1 \\ \boldsymbol{D}_2 \end{Bmatrix} \tag{16}
$$

where

$$
\begin{aligned}
\boldsymbol{A}_1 &= [\boldsymbol{a}_1, \boldsymbol{a}_2, \boldsymbol{a}_3, \boldsymbol{a}_4] \\
\boldsymbol{A}_2 &= [\boldsymbol{a}_5, \boldsymbol{a}_6, \boldsymbol{a}_7, \boldsymbol{a}_8] \\
\boldsymbol{B}_1 &= [\boldsymbol{b}_1, \boldsymbol{b}_2, \boldsymbol{b}_3, \boldsymbol{b}_4] \\
\boldsymbol{B}_2 &= [\boldsymbol{b}_5, \boldsymbol{b}_6, \boldsymbol{b}_7, \boldsymbol{b}_8] \\
\langle e^{s^* x_3} \rangle &= \mathrm{diag}[e^{s_1 x_3}, e^{s_2 x_3}, e^{s_3 x_3}, e^{s_4 x_3}, e^{-s_1 x_3}, e^{-s_2 x_3}, e^{-s_3 x_3}, e^{-s_4 x_3}]
\end{aligned}
\tag{17}
$$

and $\boldsymbol{D}_1$ and $\boldsymbol{D}_2$ are two 4×1 constant column matrices to be determined from boundary conditions of the plate. In other words, the first four values of the eigenvectors of matrix $\boldsymbol{N}$ form matrices $\boldsymbol{A}_1$ and $\boldsymbol{A}_2$ and last four values of the eigenvectors form matrices $\boldsymbol{B}_1$ and $\boldsymbol{B}_2$.

From Eq. (16), it can be shown that the constant column matrices, $\boldsymbol{D}_1$ and $\boldsymbol{D}_2$, can be solved for any point within layer j as follows:

$$
\begin{Bmatrix} \boldsymbol{D}_1 \\ \boldsymbol{D}_2 \end{Bmatrix}_j = \langle e^{s^*(x_3 - x_3^{(j)})} \rangle^{-1} \begin{bmatrix} \boldsymbol{A}_1 & \boldsymbol{A}_2 \\ \boldsymbol{B}_1 & \boldsymbol{B}_2 \end{bmatrix}^{-1} \begin{Bmatrix} \boldsymbol{u} \\ \boldsymbol{t} \end{Bmatrix}_{x_3} \tag{18}
$$

where s^* are all the eigenvalues of layer j and $x_3^{(j)} \le x_3 \le x_3^{(j+1)}$. Letting x_3 be $x_3^{(j)}$ and $x_3^{(j+1)}$, the column matrices, in the respective cases, are written as

$$\begin{Bmatrix} \boldsymbol{D}_1 \\ \boldsymbol{D}_2 \end{Bmatrix}_j = \begin{bmatrix} \boldsymbol{A}_1 & \boldsymbol{A}_2 \\ \boldsymbol{B}_1 & \boldsymbol{B}_2 \end{bmatrix}^{-1} \begin{Bmatrix} \boldsymbol{u} \\ \boldsymbol{t} \end{Bmatrix}_{x_3^{(j)}} = \langle e^{s^* h_j} \rangle^{-1} \begin{bmatrix} \boldsymbol{A}_1 & \boldsymbol{A}_2 \\ \boldsymbol{B}_1 & \boldsymbol{B}_2 \end{bmatrix}^{-1} \begin{Bmatrix} \boldsymbol{u} \\ \boldsymbol{t} \end{Bmatrix}_{x_3^{(j+1)}} \tag{19}$$

where h_j is the thickness of layer j given by Eq. (5). Accordingly, the displacement vector $\boldsymbol{u}$ and traction vector $\boldsymbol{t}$ on the upper interface $x_3 = x_3^{(j+1)}$ can be expressed in terms of those on the lower interface $x_3 = x_3^{(j)}$ of layer j as

$$\begin{Bmatrix} \boldsymbol{u} \\ \boldsymbol{t} \end{Bmatrix}_{x_3^{(j+1)}} = \begin{bmatrix} \boldsymbol{A}_1 & \boldsymbol{A}_2 \\ \boldsymbol{B}_1 & \boldsymbol{B}_2 \end{bmatrix} \langle e^{s^* h_j} \rangle \begin{bmatrix} \boldsymbol{A}_1 & \boldsymbol{A}_2 \\ \boldsymbol{B}_1 & \boldsymbol{B}_2 \end{bmatrix}^{-1} \begin{Bmatrix} \boldsymbol{u} \\ \boldsymbol{t} \end{Bmatrix}_{x_3^{(j)}} \tag{20}$$

Since the displacement $\boldsymbol{u}$ and traction $\boldsymbol{t}$ are assumed to be continuous across the interfaces, Eq. (20) can be applied repeatedly allowing the physical quantities to propagate from the bottom surface $x_3 = 0$ to the top surface $x_3 = H$ of the multilayered 1D QC plate. Therefore

$$\begin{Bmatrix} \boldsymbol{u} \\ \boldsymbol{t} \end{Bmatrix}_H = \boldsymbol{P}_N(h_N)\boldsymbol{P}_{N-1}(h_{N-1})\ldots\boldsymbol{P}_2(h_2)\boldsymbol{P}_1(h_1) \begin{Bmatrix} \boldsymbol{u} \\ \boldsymbol{t} \end{Bmatrix}_0 \tag{21}$$

where

$$\boldsymbol{P}_j(h_j) = \begin{bmatrix} \boldsymbol{A}_1 & \boldsymbol{A}_2 \\ \boldsymbol{B}_1 & \boldsymbol{B}_2 \end{bmatrix} \langle e^{s^* h_j} \rangle \begin{bmatrix} \boldsymbol{A}_1 & \boldsymbol{A}_2 \\ \boldsymbol{B}_1 & \boldsymbol{B}_2 \end{bmatrix}^{-1} \text{ for } j = 1, 2, \ldots, N \tag{22}$$

is defined as the propagator matrix of layer j. For a multilayered plate, each layer will have a propagator matrix defined. Hence, this formulation simplifies the analysis of plates composed of many layers with different material properties in each layer.

For free vibration analysis, the boundary conditions are given as traction free at the top and bottom surfaces of the plate. Applying these boundary conditions to Eq. (21), we have

$$\begin{Bmatrix} \boldsymbol{u} \\ \boldsymbol{0} \end{Bmatrix}_H = \begin{bmatrix} \boldsymbol{C}_1 & \boldsymbol{C}_2 \\ \boldsymbol{C}_3 & \boldsymbol{C}_4 \end{bmatrix} \begin{Bmatrix} \boldsymbol{u} \\ \boldsymbol{0} \end{Bmatrix}_0 \tag{23}$$

where $\boldsymbol{C}_i$ are the submatrices of the product of the propagator matrices for the multiple layers. From Eq. (23), the natural frequencies are found by letting the determinant of $\boldsymbol{C}_3$ be zero. It is noted that in the solution process, the matrix $\boldsymbol{N}$ as given in Eq. (15) is generated for each layer of a multilayered plate with an unknown value of ω.

4 Natural Frequencies and Mode Shapes

This section illustrates the free vibration response of 1D QCs layered plates under simply supported lateral boundary conditions using the novel approach proposed in this paper. Four different simply supported plates are considered: a homogenous crystal plate made of $BaTiO_3$; a homogenous QC plate made of Al-Ni-Co; a sandwich plate $BaTiO_3$/Al-Ni-Co/$BaTiO_3$ (called C/QC/C); and another sandwich plate Al-Ni-Co/$BaTiO_3$/Al-Ni-Co (called QC/C/QC).

Elastic constants of QCs are typically measured through methods of neutron scattering, X-ray diffraction, or nuclear-magnetic resonance [2]. Although there is no measured value of the phonon–phason coupling elastic constants in Al-Ni-Co, the kinetic coefficient of the phason field could be used in its place [5]. For Al-Ni-Co as a 1D hexagonal QC with Laue class 10, its density and elastic constants are listed in Table 1. The density and elastic constants for crystal $BaTiO_3$ are listed in Table 2.

It is imperative to note that in classical crystalline materials, only phonon field exists and there is no phason field [4,5]. Thus in Eq. (3), both the phason elastic constants K_i and phonon–phason coupling elastic constants R_i should be zero. Since a zero value of the phason elastic constant K_i in the crystal layer would cause singularity in the involved 4×4 matrices, a small K_i value (10^{-8} of the corresponding K_i value in QC layer) is used in the crystal layer. Also, the phason components in the displacement vector given by Eq. (6) and traction vector given by Eq. (7) should be zero. In doing so, the homogenous crystal plate becomes a special case of the homogeneous 1D QC plate.

To generalize the application of the numerical examples, the dimensions and material properties of the plates are normalized. The maximum lateral dimension denoted as L_{max} is used to normalize the dimensions of the plate. For both the homogenous crystal and QC plates considered, the normalized thickness of the plate is $H/L_{max} = 0.3$. For the two sandwich cases, the three layers are assumed to have equal normalized thickness of 0.1 making the total normalized thickness of the sandwich plate $H/L_{max} = 0.3$. We further assume that the lateral dimensions of the plates are equal and their normalized values are $L_1/L_{max} \times L_2/L_{max} = 1.0 \times 1.0$. In addition, the phonon, phason, and phonon–phason coupling elastic constants are normalized by C_{max} with C_{max} being the maximum elastic constant in the entire plate. The maximum density in the entire plate denoted as ρ_{max} is used to normalize the densities of each material layer.

Listed in Table 3 are the first eight natural frequencies of the four plate cases considered. The values are normalized as [19]

Table 1 Material properties of QC Al-Ni-Co [6]

Crystal properties of Al-Ni-Co		
Phonon elastic constants (10^{10} N/m^2)		
$C_{11} = 23.433$	$C_{12} = 5.741$	$C_{13} = 6.663$
$C_{33} = 23.222$	$C_{44} = 7.019$	$C_{66} = 8.846$
Phason elastic constants (10^{10} N/m^2)		
$K_1 = 12.2$	$K_2 = 2.4$	
Phonon–phason coupling elastic constants (10^{10} N/m^2)		
$R_1 = 0.8846$	$R_2 = 0.8846$	$R_3 = 0.8846$
Density		
$\rho = 4.186 \times 10^3$ kg/m^3		

Table 2 Material properties of crystal $BaTiO_3$ [16]

Crystal properties of $BaTiO_3$		
Phonon elastic constants (10^{10} N/m^2)		
$C_{11} = 16.6$	$C_{12} = 7.7$	$C_{13} = 7.8$
$C_{33} = 16.2$	$C_{44} = 4.3$	$C_{66} = 4.45$
Phason elastic constants		
$K_1 = K_2 = 0$		
Phonon–phason coupling elastic constants		
$R_1 = R_2 = R_3 = 0$		
Density		
$\rho = 5.8 \times 10^3$ kg/m^3		

Table 3 Normalized natural frequencies Ω of various plates investigated

Mode	C Only	QC Only	C/QC/C	QC/C/QC
1	1.18814303	1.27620020	1.09302314	1.34615671
2	2.30033364	2.72975953	2.33240979	2.75146696
3	3.83027810	4.22377419	3.76467035	4.25663661
4	5.80500015	6.34816968	5.50848985	6.42245243
5	6.70177439	7.18942970	6.21371580	7.49126055
6	9.54302478	9.87617597	9.06656633	10.04473201
7	10.90493019	11.78313507	10.28799978	11.91426946
8	12.28258976	12.81437922	11.45737354	13.03354988

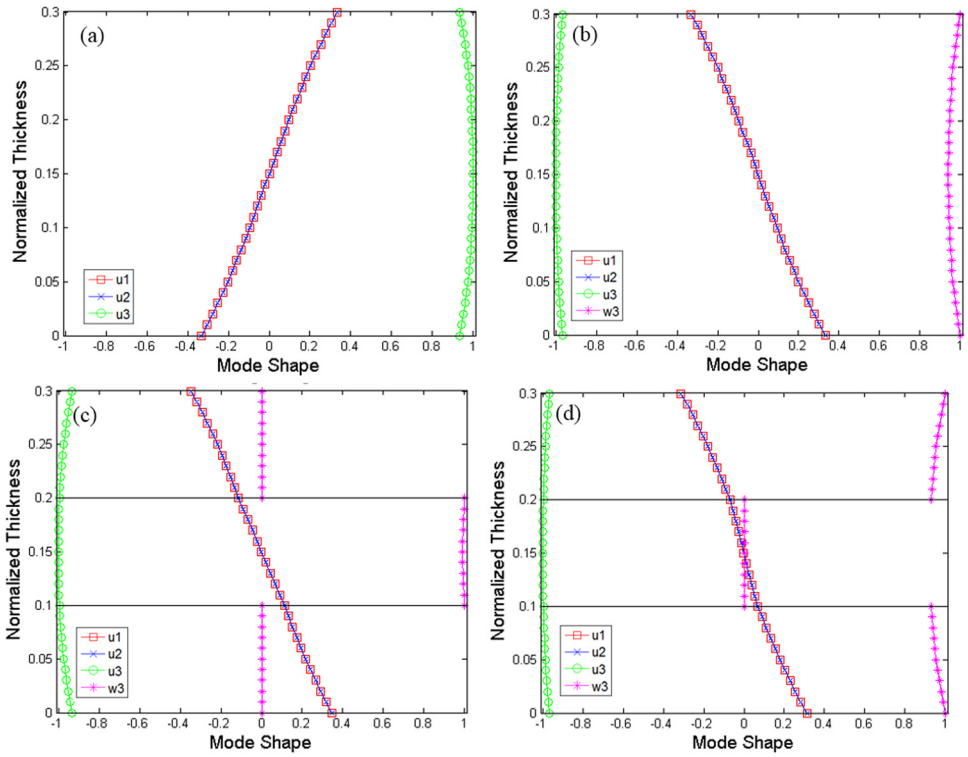

Fig. 2 First mode shape for (*a*) crystal homogenous plate with normalized natural frequency $\Omega = 1.19$, (*b*) QC homogenous plate with $\Omega = 1.28$, (*c*) sandwich plate C/QC/C with $\Omega = 1.09$, and (*d*) sandwich plate QC/C/QC with $\Omega = 1.35$

$$\Omega = \omega L_{\max} / \sqrt{C_{\max}/\rho_{\max}} \tag{24}$$

From Table 3, it can be observed that on the same mode, the QC/C/QC sandwich plate has the largest natural frequencies compared with the other plates. On the same mode, the natural frequencies of the homogeneous crystal plate are closest in value to those of the C/QC/C sandwich plate. With the exception of the second mode, the C/QC/C sandwich plate has smaller natural frequencies compared with the homogenous crystal plate. Furthermore, the natural frequencies of the homogeneous QC plate are closest in value to those of the QC/C/QC sandwich plate on the same mode. Unlike the previous case, the QC/C/QC sandwich plate has higher natural frequencies compared with the homogenous QC plate. This demonstrates clearly the interesting effect of stacking sequences in layered plates on the natural frequencies.

To illustrate the free vibration response of phonon and phason fields, mode shapes (in the thickness direction) corresponding to the first four modes given in Table 3 are, respectively, plotted in Figs. 2–5. The point of analysis is located on the plate at $(x_1,x_2)/L_{\max} = (0.75,0.75)$. In these figures, phonon displacements are normalized by the maximum absolute value in the entire thickness of the plate and the phason displacement is normalized by the corresponding maximum absolute value provided it is nonzero.

Figure 2 shows the antisymmetric mode shapes corresponding to the first mode. The phonon modal displacements u_1 and u_2 are equal in value in each plate case. Figures 2(*b*)–2(*d*), respectively, for the homogenous QC plate, C/QC/C sandwich plate, and QC/C/QC sandwich plate, display similar phonon modal displacements. However, these plates show an opposite response of the phonon displacement to that of the homogenous crystal plate shown in Fig. 2(*a*). This indicates that the first mode for the homogenous QC plate and sandwich plate is not an elastic response.

Symmetric mode shapes corresponding to the second mode given in Table 3 are shown in Fig. 3. On this particular mode, the phonon modal displacements u_1 and u_2 are opposite in value for each given plate. Furthermore, there is no phonon displacement u_3 and no phason displacement w_3 response. From Figs. 3(*a*) and 3(*c*), which show, respectively, the modal response for the homogenous crystal plate and the C/QC/C sandwich plate, it can be seen that these two plates exhibit different orders of phonon mode shapes (second-order curve in C/QC/C versus vertical straight line in crystal plate). Thus, the response of the C/QC/C sandwich plate is still predominantly elastic but is influenced by the phonon–phason coupling due to the introduction of the middle QC layer. Also in this mode, the free vibration response of the homogenous QC plate shown in Fig. 3(*b*) is purely elastic because it exactly follows the response of the homogenous crystal plate. As for Fig. 3(*d*) for the QC/C/QC sandwich plate, it is clear that its phonon mode shapes are completely different than those of the other plates, implying the important effect of stacking sequences (QC/C/QC versus C/QC/C) and of the coupling between phonon and phason fields (crystal versus QC).

Figure 4 shows another set of symmetric mode shapes corresponding to the third mode given in Table 3. On this mode, the phonon modal displacements u_1 and u_2 are exactly the same for each studied plate. The phonon modal displacement u_3 follows a similar trend of decreasing in algebraic value from the bottom to the top of all the plate cases. It follows that the phonon modal response of the homogenous QC plate and sandwich plates is elastically dominated. However, the phonon mode shape distorts significantly in the sandwich plates due to the phonon–phason coupling and stacking sequence. Also on this mode, the phason mode shape w_3 follows a linearly decreasing trend from the bottom to the top within each QC layer. This indicates that the phason mode shape in the sandwich plates with a QC layer follows the corresponding mode shape in a homogenous QC plate.

Another set of antisymmetric mode shapes corresponding to the fourth mode are shown in Fig. 5. On this mode, phonon mode shapes u_1 and u_2 are opposite in value in each plate case. Similar to the second mode, there is no phonon displacement u_3 and no phason displacement w_3. The C/QC/C sandwich plate shown in

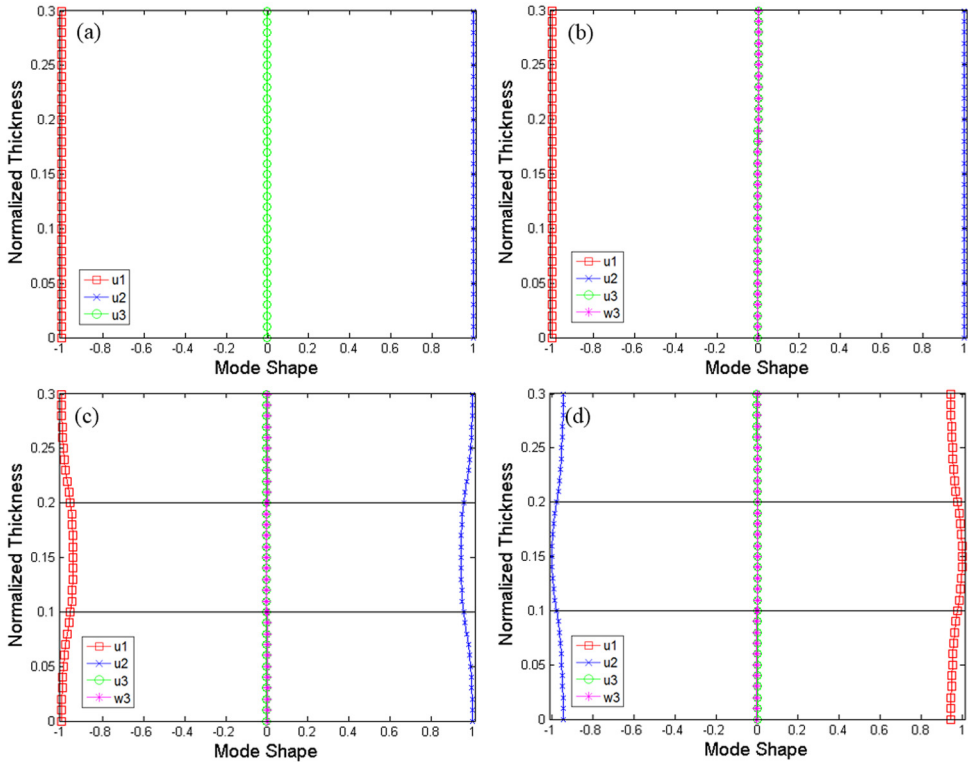

Fig. 3 Second mode shape for (*a*) crystal homogenous plate with normalized natural frequency $\Omega = 2.30$, (*b*) QC homogenous plate with $\Omega = 2.73$, (*c*) sandwich plate C/QC/C with $\Omega = 2.33$, and (*d*) sandwich plate QC/C/QC with $\Omega = 2.75$

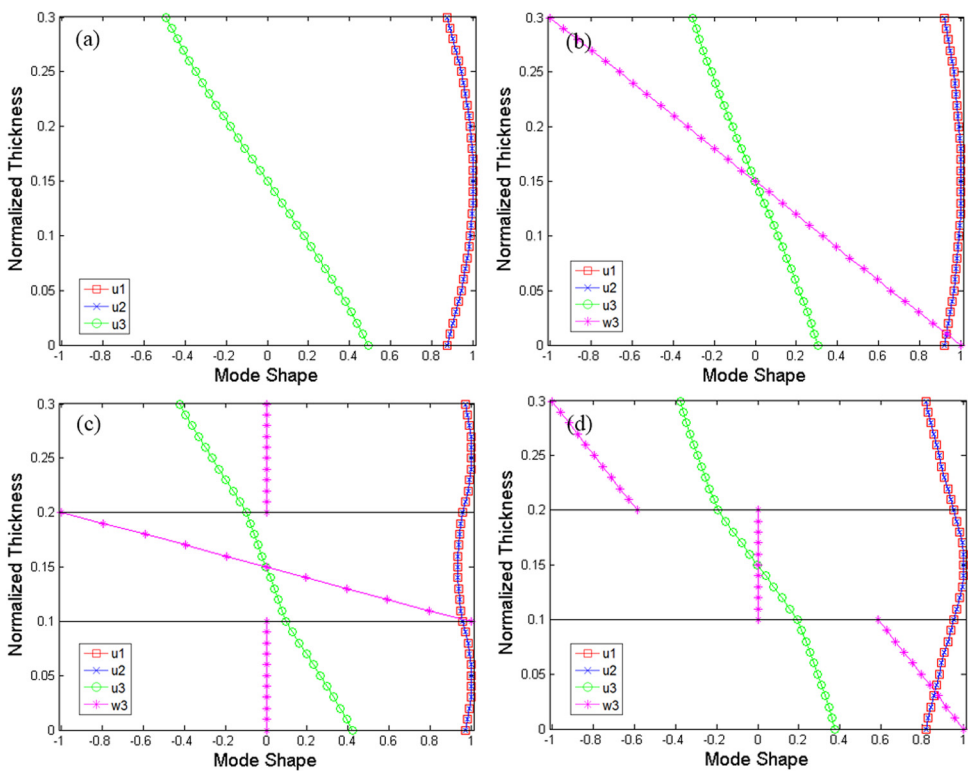

Fig. 4 Third mode shape for (*a*) crystal homogenous plate with normalized natural frequency $\Omega = 3.83$, (*b*) QC homogenous plate with $\Omega = 4.22$, (*c*) sandwich plate C/QC/C with $\Omega = 3.76$, and (*d*) sandwich plate QC/C/QC with $\Omega = 4.26$

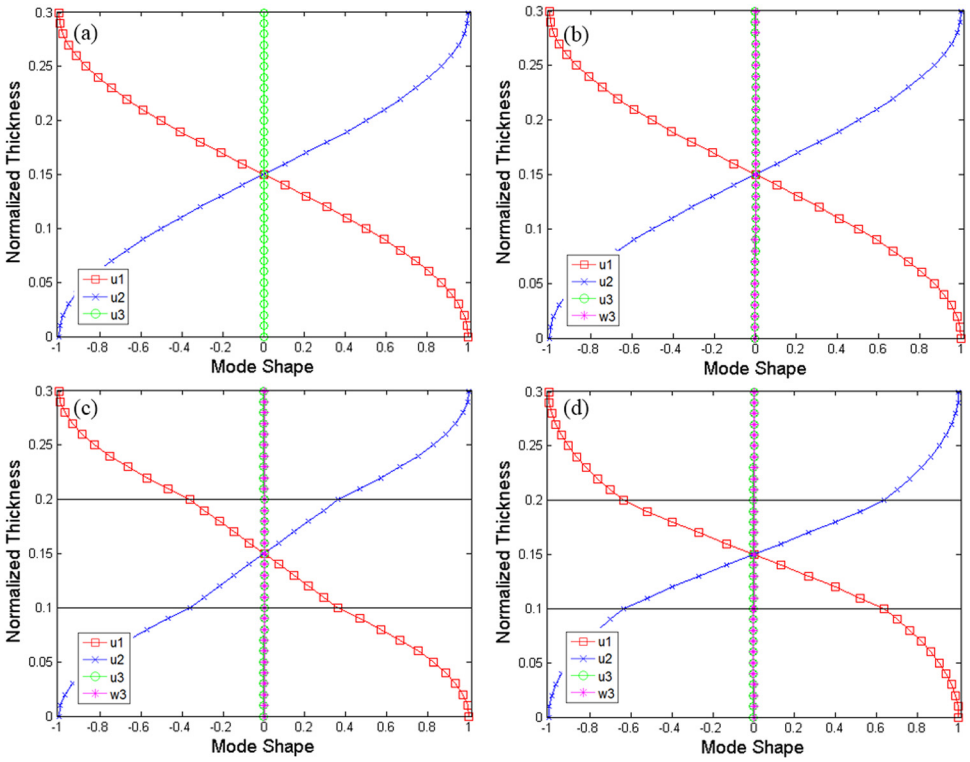

Fig. 5 Fourth mode shape for (*a*) crystal homogenous plate with normalized natural frequency $\Omega = 5.81$, (*b*) QC homogenous plate with $\Omega = 6.35$, (*c*) sandwich plate C/QC/C with $\Omega = 5.51$, and (*d*) sandwich plate QC/C/QC with $\Omega = 6.42$

Fig. 5(*c*) follows the response of the homogenous crystal plate shown in Fig. 5(*a*) with some effect of the phonon–phason coupling. Moreover, Fig. 5(*b*) for the homogenous QC plate and Fig. 5(*d*) for the QC/C/QC sandwich plate are purely elastic since the modal response is exactly the same to the crystal plate.

It is noted that from the second and fourth mode shapes shown, respectively, in Figs. 3 and 5, there is no free vibration response in the phason field. However, in the first and in the third mode shapes, shown, respectively, in Figs. 2 and 4, the homogenous QC plate and both sandwich plates exhibit a nonzero phason mode shape in QC layers. The fluctuations in phason modes are attributed to the phonon–phason coupling effect [15]. Another argument regarding the dynamic behaviour of QCs indicates phason modes are diffusive with large diffusion time [16]. The large diffusion time is due to atomic rearrangements and the insensitivity of phasons to spatial translation [5,16]. Since Bak's theory is utilized in this work, the fluctuations of phason modes are primarily attributed to the phonon–phason coupling effect.

One of the assumptions in this work includes that the displacement and traction vectors are continuous at the interface of the layers. This assumption holds with the exception of the sandwich plates, shown in Figs. 2(*c*), 2(*d*), 4(*c*), and 4(*d*), where the phason displacement is discontinuous. In these figures, the mode shape for phason displacement w_3 shows a nonzero response in QC layers and zero in crystal layers. Since phason fields do not exist in crystals, the phason components in the displacement vector given by Eq. (6) and traction vector given by Eq. (7) are explicitly set equal to zero. According to Fan et al. [20], the only continuity boundary condition in the phason field that needs to hold at the interface between QC and crystal layer is that the phason stress is equal to zero and discontinuity of the phason mode shape at the interface is attributed to the rearrangement of atomic configurations. Further investigations recently conducted by Yang et al. [21] on multilayered two-dimensional QC plates show the influence of stacking sequence on all physical properties especially at the interface.

5 Conclusions

In this work, the exact closed-form solution of free vibration for simply supported and multilayered 1D QC plates has been derived utilizing the pseudo-Stroh formulation and propagator matrix method. A homogenous crystal plate is also discussed as a special case of the derivation. Four plate cases as numerical illustrations are presented indicating the different roles that phonon and phason modes play in the dynamic analysis of QCs. With x_3-axis as the quasi-periodic direction, it is expected that phonon mode shapes for u_1 and u_2 will be either equal or opposite. The phason modal displacement w_3 will only show a response in QC layers since phason fields do not exist in crystals. However, if phonon mode shape u_3 does not show any response, the phason mode shape w_3 will neither. The fluctuation of phason modes between zero and nonzero values is also attributed to the phonon–phason coupling effect. Specifically for multilayered plates, the mode shapes will be additionally influenced by the stacking sequence. Although the current applications of QCs are limited, they possess many advantageous properties which can be greatly utilized. This work could be employed to further expand the applications of QC especially if used in layered composite materials.

Acknowledgment

The work is supported by the National Natural Science Foundation of China (No. 11172319), Chinese Universities Scientific Fund (Nos. 2011JS046 and 2013BH008), Opening Fund of State Key Laboratory of Nonlinear Mechanics, Program for New Century Excellent Talents in University (No. NCET-13-0552), and National Science Foundation for Postdoctoral Scientists of China (No. 2013M541086).

References

[1] Shechtman, D., Blech, I., Gratias, D., and Cahn, J. W., 1984, "Metallic Phase With Long-Range Orientational Order and No Translational Symmetry," Phys. Rev. Lett., **53**(20), pp. 1951–1953.

[2] Louzguine-Luzgin, D. V., and Inoue, A., 2008, "Formation and Properties of Quasicrystals," Annu. Rev. Mater. Res., **38**, pp. 403–423.

[3] Hu, C., Wang, R., and Ding, D. H., 2000, "Symmetry Groups, Physical Property Tensors, Elasticity and Dislocations in Quasicrystals," Rep. Prog. Phys., **63**(1), pp. 1–39.

[4] Ding, D. H., Yang, W. G., Hu, C. Z., and Wang, R. H., 1993, "Generalized Elasticity Theory of Quasicrystals," Phys. Rev. B, **48**(10), pp. 7003–7010.

[5] Fan, T. Y., 2011, *Mathematical Theory of Elasticity of Quasicrystals and Its Applications*, Springer, Heidelberg, Germany.

[6] Fan, T. Y., 2013, "Mathematical Theory and Methods of Mechanics of Quasicrystalline Materials," Engineering, **5**(4), pp. 407–448.

[7] Fan, T. Y., Tang, Z. Y., and Chen, W. Q., 2012, "Theory of Linear, Nonlinear and Dynamic Fracture for Quasicrystals," Eng. Fract. Mech., **82**, pp. 185–194.

[8] Farzbod, F., and Leamy, M. J., 2011, "Analysis of Bloch's Method in Structures With Energy Dissipation," ASME J. Vib. Acoust., **133**(5), p. 051010.

[9] Sladek, J., Sladek, V., and Pan, E., 2013, "Bending Analyses of 1D Orthorhombic Quasicrystal Plates," Int. J. Solids Struct., **50**(24), pp. 3975–3983.

[10] Chalak, H. D., Chakrabarti, A., Iqbal, M. A., and Sheikh, A. H., 2013, "Free Vibration Analysis of Laminated Soft Core Sandwich Plates," ASME J. Vib. Acoust., **135**(1), p. 011013.

[11] Yan, Z. Z., Zhang, Ch., and Wang, Y. S., 2013, "Elastic Wave Localization in Layered Phononic Crystals With Fractal Superlattices," ASME J. Vib. Acoust., **35**(4), p. 041004.

[12] Pan, E., 2001, "Exact Solution for Simply Supported and Multilayered Magneto-Electro-Elastic Plates," ASME J. Appl. Mech., **68**(4), pp. 608–618.

[13] Pan, E., 1997, "Static Green's Functions in Multilayered Half Spaces," Appl. Math. Model., **21**(8), pp. 509–521.

[14] Wang, R. H., Yang, W. G., Hu, C. Z., and Ding, D. H., 1997, "Point and Space Groups and Elastic Behaviors of One-Dimensional Quasicrystals," J. Phys.: Condens. Matter, **9**(11), pp. 2411–2422.

[15] Bak, P., 1985, "Symmetry, Stability and Elastic Properties of Icosahedral Incommensurate Crystals," Phys. Rev. B, **32**(9), pp. 5764–5772.

[16] Lubensky, T. C., Ramaswamy, S., and Joner, J., 1985, "Hydrodynamics of Icosahedral Quasicrystals," Phys. Rev. B, **32**(11), pp. 7444–7452.

[17] Stroh, A. N., 1958, "Dislocations and Cracks in Anisotropic Elasticity," Philos. Mag., **3**(30), pp. 625–646.

[18] Lee, J. S., and Jiang, L. Z., 1996, "Exact Electroelastic Analysis of Piezoelectric Laminae Via State Space Approach," Int. J. Solids Struct., **33**(7), pp. 977–990.

[19] Pan, E., and Heyliger, P. R., 2002, "Free Vibrations of Simply Supported and Multilayered Magneto-Electro-Elastic Plates," J. Sound Vib., **252**(3), pp. 429–442.

[20] Fan, T. Y., Xie, L. Y., Fan, L., and Wang, Q. Z., 2011, "Interface of Quasicrystals and Crystal," Chin. Phys. B, **20**(7), p. 076102.

[21] Yang, L., Gao, Y., Pan, E., and Waksmanski, N., 2014, "An Exact Solution for a Multilayered Two-Dimensional Decagonal Quasicrystal Plate," Int. J. Solids Struct., **51**(9), pp. 1737–1749.